Directing the selectivity of oxygen reduction to water by confining a Cu catalyst in a metal organic framework

Hoefnagel, M.E.; Rademaker, D.; Hetterscheid, D.G.H.

ChemSusChem

Research Article
doi.org/10.1002/cssc.202300392

Chemistry Europe
European Chemical Societies Publishing

www.chemsuschem.org

Directing the Selectivity of Oxygen Reduction to Water by Confining a Cu Catalyst in a Metal Organic Framework

Marlene E. Hoefnagel,[a] Dana Rademaker,[a] and Dennis G. H. Hetterscheid*[a]

Electrocatalysis is to play a key role in the transition towards a sustainable chemical and energy industry and active, stable and selective redox catalysts are much needed. Porous structures such as metal organic frameworks (MOFs) are interesting materials as these may influence selectivity of chemical reactions through confinement effects. In this work, the oxygen reduction catalyst Cu-tmpa was incorporated into the NU1000 MOF. Confinement of the catalyst within NU1000 steers the selectivity of the oxygen reduction reaction (ORR) towards water rather than peroxide. This is attributed to retention of the obligatory H_2O_2 intermediate in close proximity to the catalytic center. Moreover, the resulting NU1000|Cu-tmpa MOF shows an excellent activity and stability in prolonged electrochemical studies, illustrating the potential of this approach.

Introduction

Catalysis will contribute largely to modernization of the chemical industry as it facilitates making carbon neutral fuels and making industrial chemical processes more sustainable. Electrocatalysis in specific is expected to play a key role in the replacement of fossil fuels and polluting chemistry by sustainable alternatives.[1–3] Key characteristics that make a good catalyst are activity, stability and selectivity. Porous materials, such as zeolites, porous carbon materials, covalent organic frameworks (COFs) and metal organic frameworks (MOFs) have shown to affect the selectivity by so-called confinement effects.[4–8] These confinement effects include the diffusion of substrate and arrangement of substrate relative to the catalytic center, as well as spatial arrangement of catalytic centers relative to each other.[9] Geometrical constraints caused by pore size have shown to enable enantiomeric and chiral selectivity.[10,11] Moreover, the influence of neighboring groups to the catalytic center and hydrophilicity effects can alter affinity for substrates.[12–14] MOFs in particular offer a well-defined environment that allows for a high degree of tunability.

A catalytic reaction for which directing selectivity is of great importance is the oxygen reduction reaction (ORR), which is currently limiting the efficiency of a fuel cell. The ORR can either proceed via the 4 electron reduction to water [Eq. (1)] or via a 2 electron reduction to hydrogen peroxide [Eq. (2)], which then can be further reduced to water [Eq. (3)]. Hydrogen peroxide formed during the ORR can cause significant degradation of fuel cell membranes, and its formation should be avoided.[15] With the replacement of scarce platinum for abundant first row transition metals in mind, this is a significant limitation.

$$O_2 + 4e^- + 4H^+ \rightarrow 2H_2O \quad (1)$$

$$O_2 + 2e^- + 2H^+ \rightarrow H_2O_2 \quad (2)$$

$$H_2O_2 + 2e^- + 2H^+ \rightarrow 2H_2O \quad (3)$$

Many molecular oxygen reduction catalysts have been studied in the past three decades, which are largely based on porphyrins and phtalocyanines, as well as pyridine-based chelating complexes of the first row transition metals cobalt, iron, manganese and copper.[16–22] Amongst homogeneous oxygen reduction catalysts, one of the fastest catalysts reported thus far is copper(II) tris(2-pyridylmethyl)amine (Cu-tmpa), with a TOF_{max} of 1.8×10^6 s^{-1}.[23–27] Oxygen reduction by Cu-tmpa is initiated by reduction of Cu^{II} to Cu^{I}, followed by binding of dioxygen to the Cu^{I} species in the rate determining step. Subsequently, a proton coupled electron transfer is followed by a proton transfer that releases hydrogen peroxide as an isolable intermediate [Eq. (2)]. Hydrogen peroxide is reduced by Cu-tmpa in a slower process (2.1×10^5 s^{-1}) that presumably occurs via a homolytic scission of the O–O bond at a reduced Cu^{I} site,[28] and formation of a hydroxyl radical. Further reduction leads to formation of product water.

Several methods have been reported for the immobilization of molecular catalysts in MOFs.[29] The catalyst can for example be trapped in a MOF pore that acts as a cage (the 'ship-in-a-bottle' method),[30,31] a MOF linker can act as an anchor for the catalyst, as applied in the UiO MOF series,[32,33] or the catalyst itself is the linker within the MOF, as seen in the widely applied PCN series with porphyrinic linkers.[34–37] Additionally, a molecular catalyst can be incorporated into a MOF upon coupling a functional group in the periphery of the catalyst with terminal hydroxyl ligands present on the nodes, by a procedure called solvent assisted ligand incorporation (SALI).[38–40] The stable NU1000 MOF contains free hydroxyl ligands on its Zr-nodes,

[a] M. E. Hoefnagel, D. Rademaker, Dr. D. G. H. Hetterscheid
Leiden Institute of Chemistry
Leiden University
P.O Box 9502, 2300 RA Leiden (The Netherlands)
E-mail: d.g.h.hetterscheid@chem.leidenuniv.nl

Supporting information for this article is available on the WWW under https://doi.org/10.1002/cssc.202300392

making it suitable for such a SALI approach. Incorporating a catalyst by SALI allows it to retain its structure and its dynamics, while dimerization reactions and detachment from the electrode are prevented.[41–45] Given that the catalyst flexibility is of great importance for rapid ORR catalysis at single site copper species,[46,47] the SALI method is deemed as the most optimal. So far, catalysts that have been incorporated into MOFs by SALI include a nickel catalyst for ethylene dimerization,[48] an iridium catalyst for ethylene hydrogenation,[49] an iron porphyrin for photochemical CO_2 reduction[50] and molybdenum sulfide for electrocatalytic hydrogen evolution.[51] To the best of our knowledge, no SALI-incorporated catalysts in MOFs have been studied for the oxygen reduction reaction yet. A handful of MOFs, mainly with redox active linkers, for ORR have been studied and were found to favor hydrogen peroxide as the main product.[34,37,52–54] In general the long term performance of these MOFs is mediocre; current losses of 10–50% were observed in periods over three to six hours of electrolysis, or no stability data was provided whatsoever. In this work we have incorporated a carboxylic acid modified variation of the fast oxygen reduction catalyst Cu-tmpa into the NU1000 MOF by SALI and have studied its catalytic ORR activity electrochemically. We show that the NU1000|Cu-tmpaCOOH MOF retains its catalytic performance during prolonged electrolysis experiments and recycling experiments. Moreover it forms H_2O as the ORR product selectively, showing that confinement of the catalyst within this MOF fully directs its selectivity towards water.

Results and Discussion

Synthesis of NU1000|Cu-tmpaCOOH

In order to incorporate the catalyst in the MOF pores, a tris(2-pyridylmethyl)amine (tmpa) ligand was functionalized with a carboxylic acid group by a three step synthesis (See SI for details). In the first step, the secondary alcohol of a methyl ester functionalized piconol was oxidized to an aldehyde by Dess-Martin oxidation, followed by a reductive amination to form the tripodal tmpa ligand. In the last step, the methyl ester is hydrolyzed to a carboxylic acid. The tmpaCOOH ligand was coordinated to $Cu(OTf)_2$ to obtain [Cu-tmpaCOOH(OTf)](OTf), as confirmed by elemental analysis, HRMS and EPR (SI). Moreover, Evans NMR showed an effective magnetic moment $\mu_{eff} = 1.95$, corresponding to 1 unpaired electron as expected for Cu^{II}. The 4,4′,4″,4‴-(pyrene-1,3,6,8-tetrayl)tetrabenzoic acid (TBAPy) linker and the NU1000 MOF were synthesized following literature procedures (SI). The successful formation of NU1000 was confirmed by PXRD, N_2-adsorption isotherm and SEM measurements (Figures S1–S3). The catalyst was loaded into NU1000 pores, by soaking the MOF in a 0.1 M solution of Cu-tmpaCOOH in DMF at 60 °C for 30 days, as schematically shown in Figure 1.[39] The FTIR spectrum of NU1000 after SALI (Figure S4) shows a C=O stretch peak ($\pm$1656 cm^{-1}) that is assigned to the carbonyl of the ester bond formed between the catalyst and the MOF node. The formation of NU1000|Cu-tmpaCOOH was further confirmed by ICPMS (Table S1), EPR (Figure S5) and electrochemical characterization. ICPMS samples were prepared by digesting 150 μg of MOF sample (in triplicate) in 67% nitric acid at 100 °C overnight. The concentrations of the Zr and Cu ions in ppb were determined, which were then used to determine a Zr:Cu ratio for the sample. Since each NU1000 node contains six Zr ions, this ratio could be employed to determine the amount of catalysts per node. ICPMS showed loadings that varied between 0.8 to 1.4 Cu-tmpa units per node. MOF with a catalyst loading of 1.4 was used for electrochemical experiments, unless noted otherwise.

Synthesis of NU1000|Cu(OTf)$_2$

It has previously been reported that incorporation of Cu complexes into NU1000 may generate Cu-nanoparticles, which have been shown to be active in the CO_2 reduction reaction.[55] In order to verify whether any catalysis initiated by NU1000|Cu-tmpaCOOH MOF should be attributed to Cu-nanoparticles, Cu was incorporated into NU1000 as $Cu(OTf)_2$. A Cu loading of 1.5 Cu per Zr-node was determined for this NU1000|$Cu(OTf)_2$ sample by ICPMS.

Electrochemical behavior

The activity of NU1000|Cu-tmpaCOOH towards electrochemical O_2 reduction was studied by cyclic voltammetry (CV) (Figure 2a and 2b) and chronoamperometry (CA) (Figure 2c). An ink containing the MOF, carbon black (ratio 2:1), Nafion and acetone was dropcasted onto a glassy carbon working electrode with a radius of 2 mm. In total 150 μg of MOF was dropcasted, and the ink allowed to dry for 15 minutes before inserting the electrode in the electrolyte solution and starting

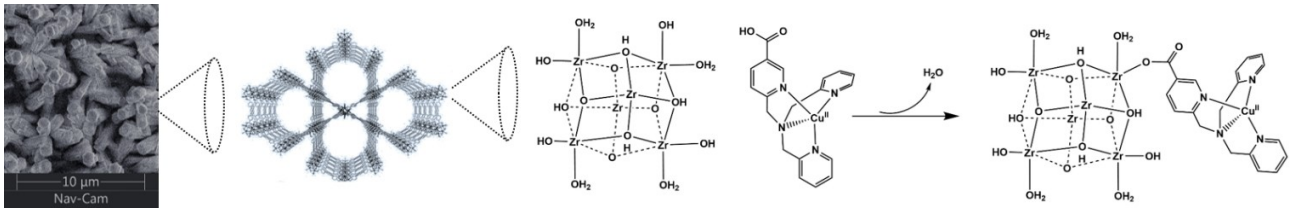

Figure 1. Schematic representation of solvent assisted ligand incorporation (SALI) of the Cu-tmpaCOOH catalyst into the NU1000 MOF. The carboxylic acid moiety on the catalyst and the hydroxyl function of the node react to form an ester link. Molecular NU1000 structure reprinted with permission from reference 40.

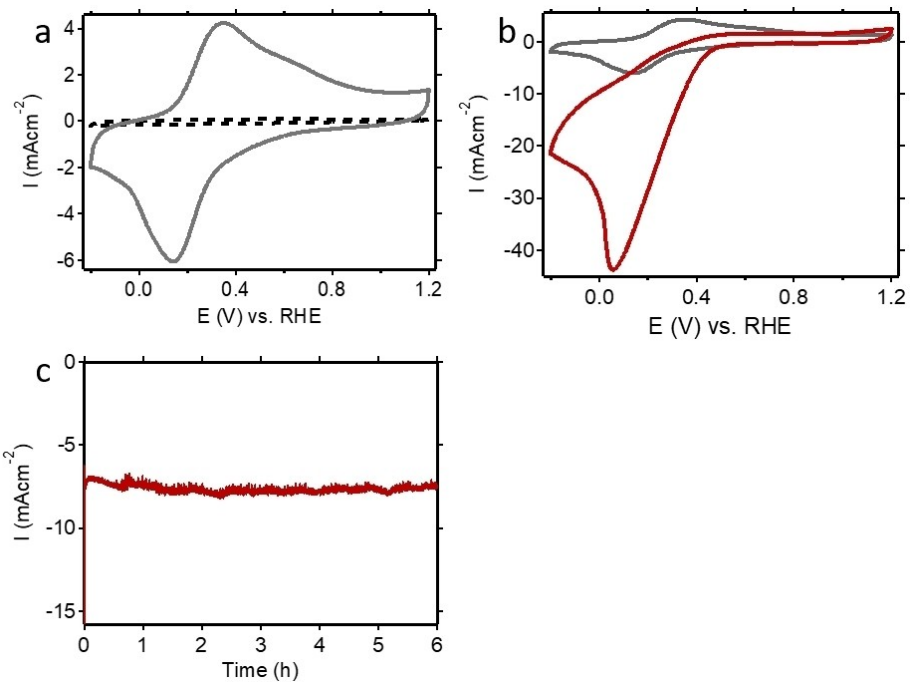

Figure 2. Cyclic voltammograms of a glassy carbon electrode under argon (a, black dotted line), NU1000|Cu-tmpaCOOH on a glassy carbon electrode under argon (a and b, grey line) and under oxygen (b, red line) and chronoamperometry at 0.3 V vs. RHE of NU1000|Cu-tmpaCOOH on a glassy carbon electrode under constant bubbling of oxygen gas (c, red line) in a 0.1 M phosphate buffer of pH 7. CVs are measured at a scan rate of 100 mV s^{-1}.

any electrochemical measurements. The CV of NU1000|Cu-tmpaCOOH in absence of oxygen, shows a quasi-reversible wave at 0.24 V vs. RHE that is assigned to the $Cu^{II/I}$ redox couple. When the Cu-tmpaCOOH catalyst is dissolved in the electrolyte rather than embedded in a MOF, a reversible wave was found at 0.24 V. vs RHE as well (Figure S6). A similar $Cu^{II/I}$ equilibrium potential of 0.21 V vs. RHE was described for Cu-tmpa.[27] The quasi-reversible character of NU1000|Cu-tmpaCOOH is expected to be caused by slow electron (Figure S7) and electrolyte transport through the framework. Slow mass and charge transport are effects previously described for electrocatalytic applications of several metal organic frameworks.[56–58] Charge transport in MOFs is governed by electron hopping coupled to cation migration and therefore greatly depends on diffusion of the cation through the framework. Integration of the reductive wave shows that 0.23 nmol electrons were transferred. Since the reduction of Cu^{II} to Cu^{I} involves a single electron, 0.23 nmol Cu centers (7.2 nmol cm^{-2}) are activated in this CV. In a homogeneous solution only a small fraction of catalyst can be activated during catalysis, while most of the catalytic species remain unaltered in the bulk solution.[59] Integration of the reductive wave in the CV of Cu-tmpaCOOH under argon taken with the catalyst dissolved in the electrolyte shows that 3.19 pmol (0.1 nmol cm^{-2}) Cu centers are activated, which illustrates the increase in activated Cu centers when immobilized in a MOF on an electrode. By immobilization of homogeneous catalysts in MOFs a significant larger number of catalytic sites can be activated, and a significant lower number of catalytic sites remains unaffected during electrochemical experiments and applications. Under an oxygen atmosphere, a catalytic wave with an onset potential ($i_p/i_{cat} \geq 2$) of 0.33 V vs. RHE appears. The catalytic wave reaches a reductive peak current density slightly larger than -40 mA cm^{-2}. Even though caution should be taken when comparing current densities of vastly different catalytic systems, a reductive current density of -40 mA cm^{-2} is competitive with the state of the art of oxygen reduction MOFs. Iron and cobalt porphyrin PCN MOFs with catalysts as every linker reached current densities of -2 mA cm^{-2}, albeit at a more positive potential of 0.8 V vs. RHE,[34,37] while a zinc MOF obtained -2.5 mA cm^{-2}.[54] Copper catalysts directly attached to, or dropcasted on electrodes, obtained current densities of -0.6 mA cm^{-2} and -5 mA cm^{-2}, respectively.[60,61] In case of NU1000|Cu-tmpaCOOH the peak current of the catalytic wave is directly proportional to catalyst loading in the MOF for the two different MOF batches used in this work (S8). Chronoamperometry (CA) was measured at 0.3 V vs. RHE for 6 hours under constant bubbling of O_2. CVs after CA (Figure S9) show that a new, irreversible redox couple has appeared and the peak belonging to the original redox couple has decreased. Additionally, ICPMS analysis of the dropcast shows lower amounts of Cu to be present in the MOF after the CA experiment compared to ICPMS analysis before the measurement (Table S1). Both observations can be explained by leaching of Cu from the MOF.[42,62,63] The additional redox couple measured after CA shows a great similarity with the redox couple measured previously for NU1000 with Cu nanoparticles,[55] as well as NU1000|$Cu(OTf)_2$ (Figure S10). This suggests that Cu particles are formed during the catalytic reaction. However, the catalytic performance of NU1000|$Cu(OTf)_2$ for both the oxygen and hydrogen peroxide reduction is

significantly lower than that of NU1000|Cu-tmpaCOOH. This suggests that the tmpaCOOH ligand is essential for catalytic activity.

Recycling experiments (Figure S11) show stable catalytic current densities of –4.5 mA cm^{-2} that could be obtained with the same electrode in five consecutive days. This illustrates that the catalytic activity of NU1000|Cu-tmpaCOOH can be maintained despite some leaching of copper. The catalytic signal of NU1000|Cu-tmpaCOOH is exceptionally stable compared to the PCN MOFs mentioned before, which were shown to have a significant loss of activity over 3–6 hours of chronoamperometry experiments. The concentration of formed H_2O_2 in presence of NU1000|Cu-tmpaCOOH was measured in fivefold with a reflectometer and reflectometer peroxide-test strips. After 6 hours, a H_2O_2 concentration of 0.21 μmol was found, with a standard deviation of 0.02 μmol of two separate 6 h CA measurements. The H_2O_2 concentration of 0.21 μmol was obtained with a current density of –7.5 mA cm^{-2} for 6 hours and translates to a faradaic efficiency (FE) that lies below 1%. As only a small portion of the current eventually ends up in H_2O_2, the ORR by this MOF is expected to favor water as the ORR product.

Rotating Disk Electrode (RDE) and Rotating Ring Disk Electrode (RRDE) measurements were performed to further investigate the selectivity of the ORR. Cyclic voltammograms at rotation speeds ranging from 400 rpm (Figure 3a, black line) to 2800 rpm (Figure 3a, dark red line) were measured and the limiting currents (at −0.35 V vs. RHE) were plotted in a Koutecky-Levich (K-L) diagram (Figure 3b). The electron transfer number (n) was calculated using the (K-L) equation (SI).[37,64] Solving this equation (see SI) resulted in $n = 4.3$, which indicates that 4 electrons are transferred per O_2 molecule and illustrates that H_2O is the main product of the ORR. A similar value of $n = 4.4$ was found for Cu-tmpaCOOH in solution (Figure S12). RRDE experiments with a Pt disk with the same size were shown to give a limiting current of –7 mA cm^{-2} in previous work.[27] As platinum is known to transfer four electrons to form water as the only product of oxygen reduction, finding similar limiting currents in case of Pt and NU1000|Cu-tmpaCOOH is in good agreement with the observed n-values. The amount of H_2O_2 produced was quantitatively analyzed by RRDE (Figure 3c, SI) with a glassy carbon disk (0.1963 cm^2) and a platinum ring (0.4398 cm^2). The currents measured at the ring (I_r) and disk (I_d) were used to calculate the FE for H_2O_2 as shown in Equation (4):

$$\mathrm{FE}\ (H_2O_2)\ \% = (200\, I_r/\mathrm{N})\ (I_d + I_r/\mathrm{N})^{-1} \quad (4)$$

Where N is the collection efficiency of H_2O_2 at the ring. A maximum faradaic efficiency of 10% for H_2O_2 in both CV and CA (at 0.3 V vs. RHE) measurements was found. The FE (H_2O_2) values found for RRDE and for directly measuring H_2O_2 concentration are significantly lower than values of 75–90% previously found for Cu-tmpa in solution,[27] and 45% for Cu-tmpaCOOH in solution (Figures 4 and S12). The relatively lower quantity of H_2O_2 observed for NU1000|Cu-tmpaCOOH is likely the result of either no H_2O_2 being formed and the ORR proceeding via a direct 4 electron reduction towards water [Eq. (1)], or as the result of fast follow up reactions involving the H_2O_2 formed [Eqs. (2), (3) and (5)].

$$2H_2O_2 \rightarrow 2H_2O + O_2 \quad (5)$$

In order to investigate whether NU1000|Cu-tmpaCOOH is able to reduce any H_2O_2 that is formed, CV and CA of H_2O_2 reduction were measured (Figure 5) and the H_2O_2 concentrations before and after CA were determined with reflectometry

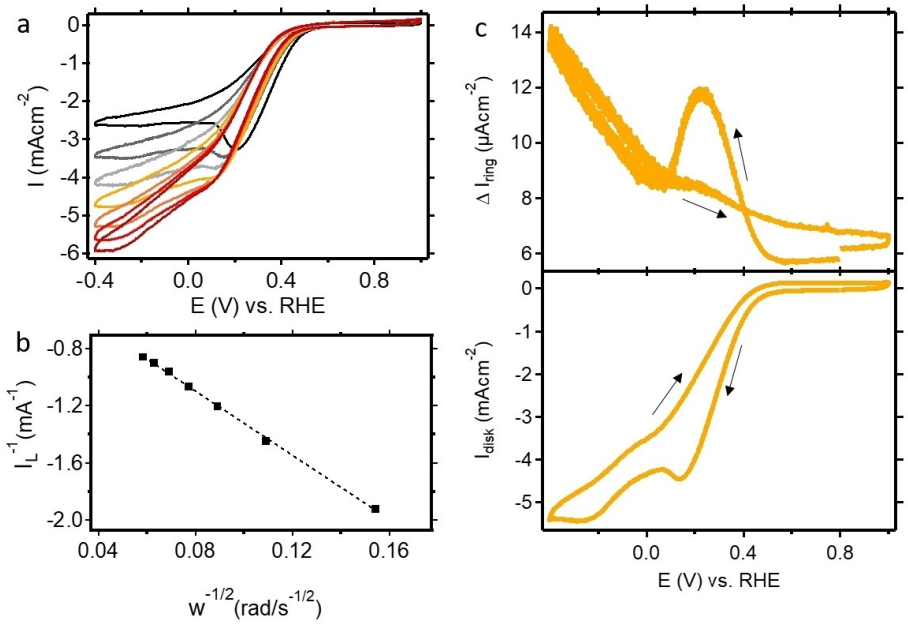

Figure 3. RDE cyclic voltammograms of NU1000|Cu-tmpaCOOH at scan rates ranging from 400 rpm (a, black line) to 2800 rpm (dark red line), Koutecky-Levich plot (b) of datapoints at −0.35 V vs. RHE ($R^2 = 0.999$) and RRDE cyclic voltammograms at 1600 rpm (c, ring current and d, disk current) at a scan rate of 50 mV s^{-1}. 100 μg of MOF with 0.8 catalysts per node was dropcasted for this experiment.

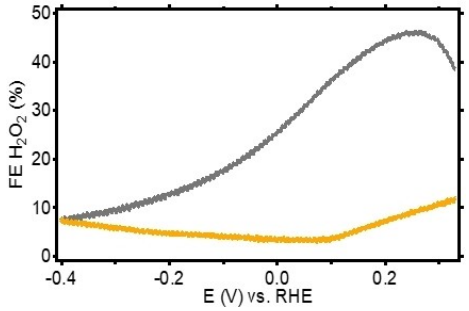

Figure 4. Faradaic efficiency for H_2O_2 in the ORR by 0.3 mM Cu-tmpaCOOH (grey line) and NU1000|Cu-tmpaCOOH (yellow line) as determined by RRDE experiments in Figures 3 and S10 during CV. The first scan, starting at the O_2 reduction onset at 0.33 V vs. RHE, to −0.4 V vs. RHE is shown.

(Table 1). After 60 minutes of chronoamperometry, 3 mmol of H_2O_2 was consumed, which equals transfer of 0.06 mmol electrons, according to Equation (3). However, the total charge after 60 minutes was 1.08 C, which is equal to 0.01 mmol electrons transferred. In other words, the amount of H_2O_2 consumed was six fold compared to the maximum amount theoretically possible if the breakdown of H_2O_2 would only occur through electrocatalysis. This strongly suggests that the disproportionation of H_2O_2 must be taking place, as previously reported for molecular Cu catalysts.[25,65,66] Control experiments illustrate that the H_2O_2 concentration does not decrease over time in absence or in presence of the NU1000|Cu-tmpaCOOH electrode if no potential is applied. Apparently, the disproportionation of H_2O_2 only happens when a reductive potential is applied, suggesting that reduced Cu species imbedded within the MOF are responsible for this reaction.

The electrocatalytic ORR mediated by NU1000|Cu-tmpaCOOH may occur via a direct 4 electron reduction reaction (eq. 1), a mechanism proceeding via the sequential reduction of O_2 to H_2O_2 (eq. 2) followed by reduction of H_2O_2 to H_2O (eq. 3) or disproportionation of H_2O_2 (eq. 5). The first of these possible mechanisms seems unlikely, as the direct 4 electron reduction towards water requires the accumulation of 4 reductive equivalents. This seems unlikely to occur for a single site Cu-tmpa catalyst. The catalytic centers in NU1000|Cu-tmpaCOOH are confined in pores and are not in close enough proximity for dimers to form, as the node-to-node distance is larger than the size of a Cu-tmpaCOOH catalyst (Figure S13). However, it is difficult to fully rule out mobility of the Cu-centers under reductive conditions. The ORR mediated by Cu-tmpa in solution was previously shown to occur via H_2O_2 as an isolatable intermediate.[27,28] Although we cannot assume that an immobilized catalyst operates via the same pathways as in solution,[42] NU1000|Cu-tmpaCOOH and Cu-tmpaCOOH behave very similar electrochemically (Figure 2, S6). NU1000|Cu-tmpaCOOH shows the same 1st order substrate concentration dependence, as was shown for Cu-tmpa previously (Figure S14–S15).[27,28] Additionally, the disproportionation of peroxide evidently plays a role when significant concentrations of hydrogen peroxide are present. As the disproportionation of hydrogen peroxide is expected to be second order in substrate,[66] it will likely contribute more to H_2O_2 clearance at high H_2O_2 concentrations. Additionally, Foot Of the Wave Analysis (FOWA) shows that the hydrogen peroxide reduction reaction of Cu-tmpaCOOH is slightly faster ($TOF_{max} = 6.8*10^4$ ($\pm 6.1*10^3$) s^{-1}) than the oxygen reduction reaction ($TOF_{max} = 3.7*10^4$ ($\pm 1.1*10^4$) s^{-1}) at equal substrate concentrations (see SI). This is in contrast to results obtained with Cu-tmpa, where oxygen reduction is significantly faster than the further reduction of hydrogen peroxide.[27,28] This suggests that Cu-tmpa-COOH is already slightly more biased towards the production of water. Most importantly, the MOF pores form a confined environment from which reactants cannot diffuse away easily.[58] H_2O_2 diffusing out of the MOF will not be able to do so without passing several catalytic centers. The retention of formed hydrogen peroxide in the MOF pores close to the catalytic center, combined with a faster further reduction of H_2O_2 to water (compared to reduction of O_2 to H_2O_2) would result in quick clearance of formed hydrogen peroxide, explaining the low amounts of hydrogen peroxide observed in our measurements. This was particularly evident from the stationary bulk electrolysis experiments. Overall we can conclude that the confinement of the Cu catalyst in NU1000 pores directs the oxygen reduction reaction towards the selective production of water.

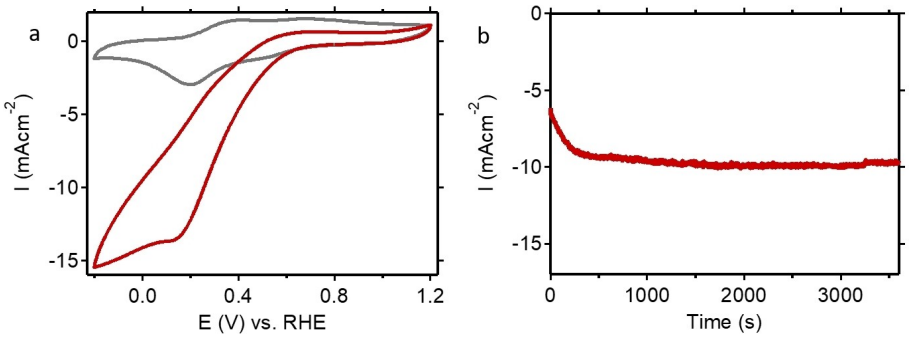

Figure 5. Cyclic voltammograms of NU1000|Cu-tmpaCOOH on a glassy carbon electrode under argon without (a, grey line) and with 7.5 mM H_2O_2 (a, red line) and chronoamperometry (b) at 0.3 V vs. RHE of NU1000|Cu-tmpaCOOH on a glassy carbon electrode in presence of 7.5 mM H_2O_2. CVs are measured at a scan rate of 100 mV s^{-1}.

Table 1. Concentrations of hydrogen peroxide in electrolyte solutions before and after H_2O_2 reduction. Concentration values are an average of four measurements with an Rqflex 20 reflectometer and reflectometer 0.2–20 mg L^{-1} peroxide-test strips.

Electrolyte solution	H_2O_2 concentration (mM)
solution at start	10.6 (±0.3)
solution after 60 minutes CA at 0.3 V vs. RHE	7.6 (±0.05)
solution after 60 minutes	10.9 (±0.2)
solution after 60 minutes exposure to a **NU1000**|**Cu-tmpaCOOH** electrode, no potential applied	10.6 (±0.3)

Conclusions

The homogeneous oxygen reduction catalyst Cu-tmpaCOOH was incorporated in the NU1000 metal organic framework by solvent assisted ligand incorporation (SALI). The resulting MOF NU1000|Cu-tmpaCOOH selectively reduces oxygen to water, with excellent catalytic rates and overall stability of the catalytic reaction. Hydrogen peroxide is a likely intermediate, yet its concentration does not build up because of its retention in the MOF pores and fast hydrogen peroxide breakdown mediated by the MOF incorporated catalyst. With this we have demonstrated that the confinement of a catalyst and substrate in MOF pores enables one to steer the oxygen reduction reaction (ORR) selectivity to a large degree. Ultimately, we show that the selectivity of electrochemical reactions can be directed without conceding on the catalytic activity or stability by incorporating a molecular catalyst into a MOF, which offers potential for a wide variety of electrochemical conversions that are relevant to the energy transition.

Experimental Section

Materials and characterization

Chemicals were purchased from commercial suppliers and used without further purification. DCM and CH_3CN were dried using a PureSolve 400 solvent dispenser. Other dry solvents (dichloroethane, EDC, dioxane) were dried on molecular sieves (3 Å) and degassed by bubbling N_2 for 15 min. Reaction flasks were degassed by 3 vacuum/N_2 cycles. Phosphate buffer was prepared using NaH_2PO_4 (Suprapur®, Merck) and Na_2HPO_4 (Suprapur®, Merck). Elemental analysis was performed by Mikroanalytisches Laboratorium Kolbe. Milli-Q Ultrapure grade water (>18.2 MΩ cm resistivity) was used for all electrochemical experiments and for the preparation of buffer. Hydrogen peroxide quantification was performed using a Rqflex 20 reflectometer purchased from Sigma Aldrich and reflectometer 0.2–20 mg L^{-1} peroxide-test strips (0.2–20 mg L^{-1} concentration range with a standard deviation of 0.2 mg L^{-1}) purchased from VWR avantor. 5.0 grade H_2, O_2 and Ar gasses were purchased from Linde. ^1H and ^{13}C NMR spectra were measured using a Bruker AV400 MHz spectrometer. Powder XRD spectra were measured on a Rigaku Miniflex II desktop X-ray diffractometer with 0.05° steps and a speed of 1° min^{-1}. N_2-adsorption isotherm was measured on a Belsorp II max. SEM images were recorded on a JSM-7600F field emission scanning electron microscope from Jeol, with a 20 mm working distance. FTIR spectra were measured on a Spectrum Two FT-IR spectrometer from Perkin Elmer. EPR was measured on a Bruker EMX EPR spectrometer and the temperature controlled with a variable Temperature unit BVT3000. ICPMS was measured on a NexION® 2000 ICP Mass Spectrometer from Perkin Elmer. Synthetic details can be found in the SI.

Sample preparation and electrochemistry

A PEEK encapsulated glassy carbon working electrode with 2 mm diameter (0.03142 cm^2 surface area) from Metrohm was polished for 2 minutes with DiaPro water-based diamond suspension, followed by 2 minutes with OP-S NonDry colloidal silica suspension, on a Struers LaboPol-20 polishing machine. The electrode was then sonicated in Milli-Q for 15 minutes and rinsed with acetone before dropcasting. A mixture of 2 mg NU1000|Cu-tmpaCOOH, 1 mg carbon black, 20 μL Nafion® perfluorinated resin solution in propanol and 180 μL HPLC-grade acetone was sonicated for 15 minutes and shortly vortexed. A 15 μL sample was dropcasted onto the GC electrode with a microman E M100 organic solvents pipet from Gilson. The electrode was allowed to dry for 15 minutes before use. Autolab PGSTAT 12 and Autolab PGSTAT 128N potentiostats were used in combination with Autolab NOVA software. A custom made, one compartment electrochemical cell with three electrode setup was used. All glassware was cleaned overnight in an aqueous 0.5 M H_2SO_4 solution with 1 mg mL^{-1} $KMnO_4$. Excess $KMnO_4$ was removed from the glassware with a diluted solution of H_2SO_4 and H_2O_2, followed by boiling (3×30 min.) in Milli-Q. A gold wire was used as the counter electrode, a platinum mesh electrode with H_2 bubbling was used as a reversible hydrogen reference electrode and a platinum wire was used as a condensator. The Pt mesh electrode was cleaned by boiling in Milli-Q for 15 minutes and the Au and Pt wires were cleaned by flame annealing. For R(R)DE measurements, a Pine instruments AFMSRCE modulated speed rotator, a GC disk with 5 mm diameter (0.1963 cm^2 surface area) and a Pt ring with 7.5 mm outer diameter and 6.5 inner diameter (0.4398 cm^2 surface area) were used. Phosphate buffer (0.1 M) pH = 7 was used as the electrolyte for all electrochemical measurements. Solutions were degassed by bubbling argon for 15 minutes, after which an argon flow over the solution was maintained during measurements. Solutions were saturated with 1.2 mM oxygen by bubbling 15 minutes with oxygen, after which an oxygen flow over the solution was maintained during measurements.

Supporting Information

Synthetic and characterization details, along with supplementary figures are provided in the Supporting Information. Additional references cited within the supporting information.[67–72]

Acknowledgements

The authors acknowledge Dr. Joost Willemse, Dr. Sipeng Zheng, and Leonardo Passerini for help with SEM, ICPMS, and EPR measurements respectively, and Phebe van Langevelde, Dr. Irene Regeni, Kyra Herrema and Dr. Stefania Grecea for scientific discussions. The authors acknowledge NWO for financial support (grant number 739.017.003).

Conflict of Interests

The authors declare no conflict of interest.

Data Availability Statement

The data that support the findings of this study are available in the supplementary material of this article.

Keywords: confinement effects · oxygen reduction · metal organic frameworks · copper · selectivity

[1] G. Papanikolaou, G. Centi, S. Perathoner, P. Lanzafame, *ACS Catal.* **2022**, 2861–2876.
[2] S. Perathoner, G. Centi, *Catal. Today* **2019**, *330*, 157–170.
[3] G. Centi, S. Perathoner, *Catal. Today* **2022**, *387*, 216–223.
[4] Y. Wang, H. Cui, Z. W. Wei, H. P. Wang, L. Zhang, C. Y. Su, *Chem. Sci.* **2016**, *8*, 775–780.
[5] Y. Ning, M. Wei, L. Yu, F. Yang, R. Chang, Z. Liu, Q. Fu, X. Bao, *J. Phys. Chem. C* **2015**, *119*, 27556–27561.
[6] K. Hemmer, M. Cokoja, R. A. Fischer, *ChemCatChem* **2021**, *13*, 1683–1691.
[7] X. Fei, P. Wang, D. Zhang, H. Wang, Z. Wu, *ChemCatChem* **2021**, *13*, 2313–2336.
[8] V. Mouarrawis, R. Plessius, J. I. van der Vlugt, J. N. H. Reek, *Front. Chem.* **2018**, *6*, 623.
[9] X. Gong, Y. Shu, Z. Jiang, L. Lu, X. Xu, C. Wang, H. Deng, *Angew. Chem. Int. Ed.* **2020**, *59*, 5326–5331.
[10] T. Uemura, R. Kitaura, Y. Ohta, M. Nagaoka, S. Kitagawa, *Angew. Chem. Int. Ed.* **2006**, *45*, 4112–4116.
[11] M. Zheng, Y. Liu, C. Wang, S. Liu, W. Lin, *Chem. Sci.* **2012**, *3*, 2623–2627.
[12] C. T. He, L. Jiang, Z. M. Ye, R. Krishna, Z. S. Zhong, P. Q. Liao, J. Xu, G. Ouyang, J. P. Zhang, X. M. Chen, *J. Am. Chem. Soc.* **2015**, *137*, 7217–7223.
[13] J. Canivet, S. Aguado, C. Daniel, D. Farrusseng, *ChemCatChem* **2011**, *3*, 675–678.
[14] A. Corma, M. J. Díaz-Cabãas, J. L. Jordá, C. Martínez, M. Moliner, *Nature* **2006**, *443*, 842–845.
[15] J. Wu, X. Z. Yuan, J. J. Martin, H. Wang, J. Zhang, J. Shen, S. Wu, W. Merida, *J. Power Sources* **2008**, *184*, 104–119.
[16] M. L. Pegis, C. F. Wise, D. J. Martin, J. M. Mayer, *Chem. Rev.* **2018**, *118*, 2340–2391.
[17] P. Vasudevan, Santosh, N. Mann, S. Tyagi, *Transition Met. Chem.* **1990**, *15*, 81–90.
[18] J. Zhang, F. C. Anson, *J. Electroanal. Chem.* **1992**, *341*, 323–341.
[19] J. Zhang, F. C. Anson, *J. Electroanal. Chem.* **1993**, *348*, 81–97.
[20] E. A. Lewis, W. B. Tolman, *Chem. Rev.* **2004**, *104*, 1047–1076.
[21] S. Kakuda, R. L. Peterson, K. Ohkubo, K. D. Karlin, S. Fukuzumi, *J. Am. Chem. Soc.* **2013**, *135*, 6513–6522.
[22] C. C. L. McCrory, X. Ottenwaelder, T. D. P. Stack, C. E. D. Chidsey, *J. Phys. Chem. A* **2007**, *111*, 12641–12650.
[23] M. Asahi, S. I. Yamazaki, S. Itoh, T. Ioroi, *Dalton Trans.* **2014**, *43*, 10705–10709.
[24] M. Asahi, S. I. Yamazaki, S. Itoh, T. Ioroi, *Electrochim. Acta* **2016**, *211*, 193–198.
[25] M. A. Thorseth, C. S. Letko, T. B. Rauchfuss, A. A. Gewirth, *Inorg. Chem.* **2011**, *50*, 6158–6162.
[26] M. A. Thorseth, C. S. Letko, E. C. M. Tse, T. B. Rauchfuss, A. A. Gewirth, *Inorg. Chem.* **2013**, *52*, 628–634.
[27] M. Langerman, D. G. H. Hetterscheid, *Angew. Chem. Int. Ed.* **2019**, *58*, 12974–12978.
[28] M. Langerman, D. G. H. Hetterscheid, *ChemElectroChem* **2021**, *8*, 2783–2791.
[29] Y. Han, J. R. Li, Y. Xie, G. Guo, *Chem. Soc. Rev.* **2014**, *43*, 5952–5981.
[30] M. R. Di Nunzio, V. Agostoni, B. Cohen, R. Gref, A. Douhal, *J. Med. Chem.* **2014**, *57*, 411–420.
[31] P. Manna, J. Debgupta, S. Bose, S. K. Das, *Angew. Chem. Int. Ed.* **2016**, *55*, 2425–2430.
[32] B. A. Johnson, A. Bhunia, S. Ott, *Dalton Trans.* **2017**, *46*, 1382–1388.
[33] S. Pullen, S. Roy, S. Ott, *Chem. Commun.* **2017**, *53*, 5227–5230.
[34] M. O. Cichocka, Z. Liang, D. Feng, S. Back, S. Siahrostami, X. Wang, L. Samperisi, Y. Sun, H. Xu, N. Hedin, H. Zheng, X. Zou, H. C. Zhou, Z. Huang, *J. Am. Chem. Soc.* **2020**, *142*, 15386–15395.
[35] N. Kornienko, Y. Zhao, C. S. Kley, C. Zhu, D. Kim, S. Lin, C. J. Chang, O. M. Yaghi, P. Yang, *J. Am. Chem. Soc.* **2015**, *137*, 14129–14135.
[36] T. F. Liu, D. Feng, Y. P. Chen, L. Zou, M. Bosch, S. Yuan, Z. Wei, S. Fordham, K. Wang, H. C. Zhou, *J. Am. Chem. Soc.* **2015**, *137*, 413–419.
[37] W. Yan, Q. Xing, O. Guo, H. Feng, H. Liu, P. Deshlahra, X. Li, Y. Chen, *ACS Appl. Mater. Interfaces* **2022**, *14*, 50761.
[38] P. Deria, J. E. Mondloch, E. Tylianakis, P. Ghosh, W. Bury, R. Q. Snurr, J. T. Hupp, O. K. Farha, *J. Am. Chem. Soc.* **2013**, *135*, 16801–16804.
[39] P. Deria, W. Bury, J. T. Hupp, O. K. Farha, *Chem. Commun.* **2014**, *50*, 1965–1968.
[40] P. Deria, W. Bury, I. Hod, C. W. Kung, O. Karagiaridi, J. T. Hupp, O. K. Farha, *Inorg. Chem.* **2015**, *54*, 2185–2192.
[41] J. T. Hyde, K. Hanson, A. K. Vannucci, A. M. Lapides, L. Alibabaei, M. R. Norris, T. J. Meyer, D. P. Harrison, *ACS Appl. Mater. Interfaces* **2015**, *7*, 9554–9562.
[42] N. W. G. Smits, D. Den Boer, L. Wu, J. P. Hofmann, D. G. H. Hetterscheid, *Inorg. Chem.* **2019**, *58*, 13007–13019.
[43] R. Matheu, L. Francàs, P. Chernev, M. Z. Ertem, V. Batista, M. Haumann, X. Sala, A. Llobet, *ACS Catal.* **2015**, *5*, 3422–3429.
[44] P. Garrido-Barros, R. Matheu, C. Gimbert-Suriñach, A. Llobet, *Curr. Opin. Electrochem.* **2019**, *15*, 140–147.
[45] A. K. Das, M. H. Engelhard, R. M. Bullock, J. A. S. Roberts, *Inorg. Chem.* **2014**, *53*, 6875–6885.
[46] N. W. G. Smits, B. van Dijk, I. de Bruin, S. L. T. Groeneveld, M. A. Siegler, D. G. H. Hetterscheid, *Inorg. Chem.* **2020**, *59*, 16398–16409.
[47] V. Budhija, P. H. Van Langevelde, K. B. Krause, B. Cula, D. G. H. Hetterscheid, M. Schwalbe, V. Budhija, K. B. Krause, B. Cula, M. Schwalbe, P. H. Van Langevelde, D. G. H. Hetterscheid, **2023**, *26*, e202200743.
[48] S. T. Madrahimov, J. R. Gallagher, G. Zhang, Z. Meinhart, S. J. Garibay, M. Delferro, J. T. Miller, O. K. Farha, J. T. Hupp, S. T. Nguyen, *ACS Catal.* **2015**, *5*, 6713–6718.
[49] D. Yang, S. O. Odoh, T. C. Wang, O. K. Farha, J. T. Hupp, C. J. Cramer, L. Gagliardi, B. C. Gates, *J. Am. Chem. Soc.* **2015**, *137*, 7391–7396.
[50] K. Zhang, S. Goswami, H. Noh, Z. Lu, T. Sheridan, J. Duan, W. Dong, J. T. Hupp, *J. Photochem. Photobiol.* **2022**, *10*, 100111.
[51] H. Noh, C. W. Kung, K. I. Otake, A. W. Peters, Z. Li, Y. Liao, X. Gong, O. K. Farha, J. T. Hupp, *ACS Catal.* **2018**, *8*, 9848–9858.
[52] E. M. Miner, S. Gul, N. D. Ricke, E. Pastor, J. Yano, V. K. Yachandra, T. Van Voorhis, M. Dincaˇ, *ACS Catal.* **2017**, *7*, 7726–7731.
[53] X. Chen, Y. Kondo, Y. Kuwahara, K. Mori, C. Louis, H. Yamashita, *Phys. Chem. Chem. Phys.* **2020**, *22*, 14404–14414.
[54] V. Raut, B. Bera, M. Neergat, D. Das, *J. Chem. Sci.* **2021**, *133*, 1–9.
[55] C. W. Kung, C. O. Audu, A. W. Peters, H. Noh, O. K. Farha, J. T. Hupp, *ACS Energy Lett.* **2017**, *2*, 2394–2401.
[56] S. Roy, V. Pascanu, S. Pullen, G. González Miera, B. Martín-Matute, S. Ott, *Chem. Commun.* **2017**, *53*, 3257–3260.
[57] I. Stassen, N. Burtch, A. Talin, P. Falcaro, M. Allendorf, R. Ameloot, *Chem. Soc. Rev.* **2017**, *46*, 3185–3241.
[58] B. A. Johnson, A. M. Beiler, B. D. McCarthy, S. Ott, *J. Am. Chem. Soc.* **2020**, *142*, 11941–11956.
[59] D. J. Cole-Hamilton, R. P. Tooze, in *Catal. Sep. Recover. Recycl.* (Eds.: D. J. Cole-Hamilton, R. P. Tooze), Springer Netherlands, **2006**, pp. 1–8.
[60] S. Wang, X. Gao, X. Mo, D. L. Phillips, E. C. M. Tse, *ACS Catal.* **2023**, *13*, 5599–5608.
[61] M. A. Thorseth, C. S. Letko, E. C. M. Tse, T. B. Rauchfuss, A. A. Gewirth, *Inorg. Chem.* **2013**, *52*, 628–634.
[62] N. W. G. Smits, D. Rademaker, A. I. Konovalov, M. A. Siegler, D. G. H. Hetterscheid, *Dalton Trans.* **2022**, *51*, 1206–1215.
[63] B. Van Dijk, J. P. Hofmann, D. G. H. Hetterscheid, *Phys. Chem. Chem. Phys.* **2018**, *20*, 19625–19634.
[64] J. Li, Y. Chen, Y. Tang, S. Li, H. Dong, K. Li, M. Han, Y. Q. Lan, J. Bao, Z. Dai, *J. Mater. Chem. A* **2014**, *2*, 6316–6319.
[65] F. Ghiretti, *Arch. Biochem. Biophys.* **1956**, *63*, 165–176.
[66] M. Jezowska-Bojczuk, W. Leśniak, W. Bal, H. Kozlowski, K. Gatner, A. Jezierski, J. Sobczak, S. Mangani, W. Meyer-Klaucke, *Chem. Res. Toxicol.* **2001**, *14*, 1353–1362.
[67] A. F. Abdel-Magid, K. G. Carson, B. D. Harris, C. A. Maryanoff, R. D. Shah, *J. Org. Chem.* **1996**, *61*, 3849–3862.
[68] Ø. Samuelsen, O. A. H. Åstrand, C. Fröhlich, A. Heikal, S. Skagseth, T. J. O. Carlsen, H. K. S. Leiros, A. Bayer, C. Schnaars, G. Kildahl-Andersen, S.

Lauksund, S. Finke, S. Huber, T. Gjøen, A. M. S. Andresen, O. A. Økstad, P. Rongved, *Antimicrob. Agents Chemother.* **2020**, *64*, e02415–19.
[69] J. E. Mondloch, W. Bury, D. Fairen-Jimenez, S. Kwon, E. J. Demarco, M. H. Weston, A. A. Sarjeant, S. T. Nguyen, P. C. Stair, R. Q. Snurr, O. K. Farha, J. T. Hupp, *J. Am. Chem. Soc.* **2013**, *135*, 10294–10297.
[70] T. C. Wang, N. A. Vermeulen, I. S. Kim, A. B. F. Martinson, J. Fraser Stoddart, J. T. Hupp, O. K. Farha, *Nat. Protoc.* **2016**, *11*, 149–162.
[71] T. Islamoglu, K. I. Otake, P. Li, C. T. Buru, A. W. Peters, I. Akpinar, S. J. Garibay, O. K. Farha, *CrystEngComm* **2018**, *20*, 5913–5918.
[72] C. Costentin, S. Drouet, M. Robert, J. M. Savéant, *J. Am. Chem. Soc.* **2012**, *134*, 11235–11242.

Manuscript received: March 17, 2023
Revised manuscript received: June 14, 2023
Accepted manuscript online: June 16, 2023
Version of record online: August 10, 2023